Geophysical Research Letters

Effective elastic thickness of the Arabian plate: Weak shield versus strong platform

Bo Chen[1], Mikhail K. Kaban[2,3], Sami El Khrepy[4,5], and Nassir Al-Arifi[4]

[1]School of Geosciences and Info-Physics, Central South University, Changsha, China, [2]Deutsches GeoForschungsZentrum Potsdam, Potsdam, Germany, [3]Geophysical Center, IPE, Russian Academy of Sciences, Moscow, Russia, [4]Geology and Geophysics Department, King Saud University, Riyadh, Saudi Arabia, [5]National Research Institute of Astronomy and Geophysics Seismology Department, Helwan, Egypt

Abstract The fan wavelet method has been employed to calculate high-resolution maps of variations of the effective elastic thickness (EET) for the Arabian plate and surroundings. As the initial data, we use high-resolution gravity field, topography, and recent models of sedimentary basins. The western part of the plate is generally characterized by low to midvalues of EET (10–30 km) while the eastern one by high values (50 km and more in the core). This finding confirms that the pronounced asymmetry of the plate is rather associated with fundamental structural differences of the lithosphere than with a forced tilt of the plate due to the rifting in the west-southwest and subduction in the northeast. Therefore, the high topography in the western part of the plate is likely supported by relatively hot mantle that is also responsible for the decrease of EET. These results are generally in agreement with recent seismic tomography models.

1. Introduction

The Arabian Plate is one of the youngest and smallest lithospheric plates, originated ~25 Ma ago due to rifting of NE Africa along the Red Sea and Gulf of Aden. One of the most striking features is a strong asymmetry, with extensive basement exposures and elevation up to 3000 m (the Arabian shield) in the west and deep sedimentary basins (Arabian platform) in the east [e.g., *Stern and Johnson*, 2010] (Figure 1). The origin of this asymmetry is still strongly debated. According to one hypothesis, the tilt of the plate is related to marginal processes. Rifting along the Red Sea in the west and in the Gulf of Aden in the south could be responsible for the uplift of the shield, while subduction beneath the Eurasian Plate in the northeast has lead to the depression in the opposite side. According to another point of view, this difference reflects a fundamental crustal and mantle heterogeneity in the plate originated from Neoproterozoic when the lithosphere formed [*Stern and Johnson*, 2010]. Structure of the crystalline crust is generally similar in the western and eastern parts [*Gettings et al.*, 1986]. The Moho is somewhat deeper under the platform; however, this difference well correlates with thickness of sediments [*Stolk et al.*, 2013]. This fact supports the first hypothesis about the forced tilt of the plate. On the other hand, recent seismic tomography models show different structure of the upper mantle beneath the shield and the platform [*Koulakov*, 2011; *Schaeffer and Lebedev*, 2013]. It is found that seismic velocities in the upper mantle are remarkably faster in the eastern part of the plate than in the western. This difference can be related to variations of the lithosphere thickness; therefore, the hot mantle under the western part supports the uplifted shield.

Effective elastic thickness (EET) of the lithosphere is the thickness of a uniform elastic layer that would respond to applied loads in the same way as the heterogeneous lithospheric plate. EET primarily depends on thermal state and structure of the lithosphere [e.g., *Burov and Diament*, 1995]; therefore, this parameter can be directly used to assess their variations. One of the most powerful methods for determination of EET variations is based on a cross-spectral analysis of gravity and topography data [e.g., *Forsyth*, 1985; *Kirby and Swain*, 2011]. The advantage of this approach is that recent satellite missions provided for the first time globally homogeneous gravity models [e.g., *Förste et al.*, 2013], which can be used even in areas without other data. Previously, *Pérez-Gussinyé et al.* [2009] presented an EET map of the African lithosphere estimated from coherence analysis of topography and Bouguer anomaly in a sliding window. *Audet and Bürgmann* [2011] have determined global variations of EET over the continents using wavelet transforms to calculate the coherence of the gravity and topography. These studies show a west-east trend over the
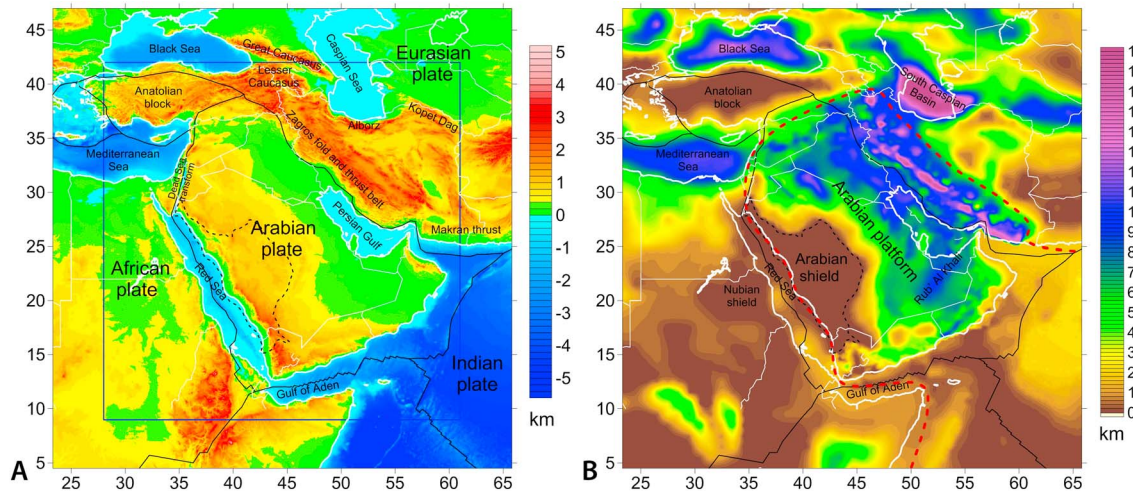
Figure 1. (a) Topography. The blue rectangle outlines the area, for which we calculate EET. (b) Thickness of sediments. For the Arabian plate and surroundings, the basement map of *Stern and Johnson* [2010] is employed. For the outer continental areas, we use the model of *Stolk et al.* [2013]. For the oceanic area, the detailed map of NOAA (NOAA, 2010, http://www.ngdc.noaa.gov/mgg/sedthick/sedthick.html) is used. The red dashed line depicts the area with high-resolution data on the thickness of sediments. The black dashed line shows the Arabian shield.

Arabian plate with the increasing effective elastic thickness, which may be related to variations of the lithosphere structure. However, higher-resolution studies are required to confirm this conclusion. In particular, the effect of weak lithosphere over the rifting zones (the Red Sea and Gulf of Aden) might be propagated to the Arabian shield. It is even more important that the topography, which is used in previous studies, represents only a part of the near-surface deformation after loading. Specifically, within the western part of Arabian plate, the topography variations are close to zero, which principally reduces reliability of the obtained results [*McKenzie*, 2003]. Density heterogeneity of sediments could significantly contribute to both surface loading and gravity anomalies [e.g., *Braitenberg et al.*, 2003].

In this study we employ the fan wavelet method [*Kirby and Swain*, 2011] to determine variations of the effective elastic thickness based on a joint analysis of the high-resolution gravity field, topography, and recent models of sedimentary basins for the Arabian plate and surroundings.

2. Fan Wavelet Coherence Method for Elastic Thickness Estimation

Wavelength dependence of the coherence between topography and gravity anomaly provides a measure of the degree of flexural compensation in response to long-term tectonic loads [e.g., *Watts*, 2001; *Audet et al.*, 2007]. The wavelength of transition from compensated to uncompensated loads is related to the characteristic flexural wavelength, which increases with increasing lithospheric rigidity (equivalently—EET) [*Forsyth*, 1985]. There exist several methods to estimate EET based on the analysis of the surface topography and gravity field. Relatively recent methods are based on the continuous wavelet transform, in which the spectral properties of a signal are localized at each grid point [e.g., *Kirby and Swain*, 2008]. Therefore, it is possible to study with relatively high-resolution spatial variations of EET (T_e). The fan wavelet method implies a series of Morlet wavelets with different azimuths [*Kirby and Swain*, 2004]. This method has been combined with the "load deconvolution" method of *Forsyth* [1985] to estimate T_e with high spatial resolution and without significant bias [*Kirby and Swain*, 2004, 2011].

The wavelet coherence between the Bouguer gravity and the topography at scale (s) and location ($\mathbf{x}$) is defined as

$$\gamma^2(s, \mathbf{x}) = \frac{\left| \langle B_{s\mathbf{x}\theta} H^*_{s\mathbf{x}\theta} \rangle_\theta \right|^2}{\langle B_{s\mathbf{x}\theta} B^*_{s\mathbf{x}\theta} \rangle_\theta \langle H_{s\mathbf{x}\theta} H^*_{s\mathbf{x}\theta} \rangle_\theta}, \tag{1}$$

where B and H are the wavelet transforms of the Bouguer gravity and the external topography after loading, respectively; s and θ are the scale and azimuth of the Morlet wavelet; the asterisk denotes complex conjugate; and $<\ >_\theta$ indicates the averaging over azimuth. The wavelet scale (s) can be converted to the equivalent Fourier wave number (k) using $k = |\mathbf{k_0}|/s$, where $|\mathbf{k_0}|$ is the central wave

number of the Morlet wavelet [*Kirby and Swain*, 2006]. Spatial resolution of the result depends on the central wave number. Four typical values of $|\mathbf{k_0}|$ (2.668, 3.081, 3.773, and 5.336) are employed to calculate EET for the Arabian plate and surroundings. These values correspond to the Morlet wavelets, whose first sidelobes are 1/16, 1/8, 1/4, and 1/2 of the central amplitude, respectively [*Kirby and Swain*, 2011]. The high $|\mathbf{k_0}|$ values yield more accurate T_e estimates for large tectonic province with a relatively uniform T_e. In contrast, the low $|\mathbf{k_0}|$ values provide better resolution and are more useful to recover detailed or small-scale T_e structures, however with the increased noise and less stability [*Kirby and Swain*, 2011; *Chen et al.*, 2015]. Therefore, we have to find a balance between these factors. This is especially important for the areas with a strong lithosphere. For example, for $T_e = 50$–60 km with the loading ratio $f = 1$, the coherence transition wavelength is about 500–600 km [*Kirby and Swain*, 2008], and the space-domain width of the wavelet (i.e., footprint) needed to resolve this anomaly is about 500–600 km for $|\mathbf{k_0}| = 2.668$ and 1000–1200 for $|\mathbf{k_0}| = 5.336$ [*Kirby and Swain*, 2011].

Reliability of the EET estimations can be assessed by calculating the normalized squared imaginary part of the free air coherency ($\overline{\Gamma}_{F,I}^2$) [*Kirby and Swain*, 2009]:

$$\Gamma_F(s, \mathbf{x}) = \frac{\langle G_{s\mathbf{x}\theta} H_{s\mathbf{x}\theta}^* \rangle_\theta}{\langle G_{s\mathbf{x}\theta} G_{s\mathbf{x}\theta}^* \rangle_\theta^{\frac{1}{2}} \langle H_{s\mathbf{x}\theta} H_{s\mathbf{x}\theta}^* \rangle_\theta^{\frac{1}{2}}}, \quad \overline{\Gamma}_{F,I}^2 = \frac{(\mathrm{Im}\Gamma_F)^2}{|\Gamma_F|^2}, \tag{2}$$

where G is the wavelet transforms of the free air gravity anomalies. As suggested by *Kirby and Swain* [2009], the coherence (and consequently EET) may be biased by "gravity noise" due to unexpressed loadings, when the maximum value of $\overline{\Gamma}_{F,I}^2$ around the Bouguer transition wavelength is larger than 0.5.

3. Initial Data

For determination of EET variations, we use the "corrected" topography, which represents a combination of the topography/bathymetry and density variations within sedimentary basins relative to the upper layer of the crystalline crust. The topography is based on the ETOPO1 model [*Amante and Eakins*, 2008] (Figure 1a). For the bathymetry, we use the model SRTM30_PLUS [*Becker et al.*, 2009], which is based on a combination of ship depth soundings and satellite altimetry. As already mentioned, density heterogeneity of sediments can substantially contribute to surface loadings [e.g., *Braitenberg et al.*, 2003]. This is especially important for the Arabian platform, where the topography signal is low. For the Arabian plate, we employ a detailed basement map [*Stern and Johnson*, 2010]. The map of NOAA is used for the oceanic area (NOAA, 2010, http://www.ngdc.noaa.gov/mgg/sedthick/sedthick.html). For the continental areas outside the Arabian plate, we use the recently published 1°×1° model for the whole Asia and surroundings [*Stolk et al.*, 2013]. The resulting map for the study area is shown in Figure 1b.

Internal density structure of sedimentary basins also varies both in horizontal and vertical directions. Based on various data (chiefly seismic, well logs, and geological), *Stolk et al.* [2013] have determined characteristic density-depth functions for different types of sedimentary basin in Asia and surroundings. In particular, for the Arabian plate, published geological cross sections [*Perotti et al.*, 2011] have been considered. This approach has been successfully used in previous works including T_e estimations [e.g., *Braitenberg et al.*, 2003; *Chen et al.*, 2013]. The corrected topography (H) is estimated as follows:

$$\begin{aligned} H &= k \cdot t + S \cdot (\rho_s - 2.67)/2.67 \\ k &= 1 \text{ for land}, \quad k = (2.67 - 1.03)/2.67 \text{ for the sea}, \end{aligned} \tag{3}$$

where S is the thickness of sediments, t is the topography, ρ_s is the vertically averaged density of sediments, and 2.67 g/cm^3 is the standard density of the uppermost crystalline crust. The corrected topography for the study area is shown in Figure 2a.

For the gravity field, we use the EIGEN-6c3stat model [*Förste et al.*, 2013], which is based on a combination of the satellite and terrestrial data. A special band-limited combination method has been applied in order to preserve the high accuracy from the satellite data in the lower-frequency band of the geopotential and to form a smooth transition to the high-frequency information obtained from surface data. The model is complete to a degree/order 1949 in terms of spherical harmonic coefficients, which approximately corresponds to the spatial resolution 5′×5′ of the gravity disturbances. The Bouguer correction (for both, continental and ocean parts) has been computed using ETOPO1 data for elevations [*Amante and Eakins*, 2008] and the data of
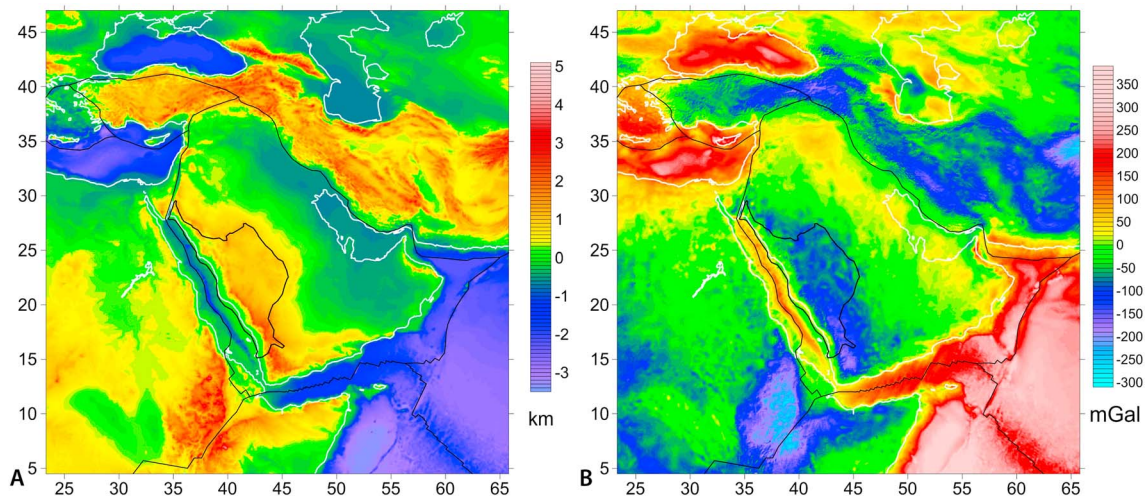
Figure 2. (a) Corrected topography combining the effects of topography/bathymetry and sediments; density is adjusted to 2.67 g/cm^3 (see text). (b) Gravity disturbances corrected for the effects of topography/bathymetry and sediments.

Becker et al. [2009] for bathymetry. The computations are limited to the radius 222 km around each point, and all spherical effects are taken into account. In addition, the gravity effect of sediments has been estimated relative to a standard density of 2.67 g/cm^3 in the same way as in *Kaban and Mooney* [2001]. This effect has been removed from the Bouguer gravity disturbances. The corrected field is shown in Figure 2b. These data are used for computation of EET variations for the Arabian plate and surroundings.

For interpretation, we also need to know the Moho depth, which is the main density boundary within the lithosphere. For these purposes, we use the Moho model from *Stolk et al.* [2013]. For calculations, all the data have been resampled into 10×10 km grids using the transverse Mercator projection.

Uncertainty of the initial data might also influence the calculated EET. For the Moho depth, *Pérez-Gussinyé et al.* [2009] and *Kirby and Swain* [2009] have demonstrated that possible uncertainties (± 4 km in the employed model of *Stolk et al.* [2013]) have an insignificant effect on the recovered EET. Also, the model of sediments does not include local details. *Mooney and Kaban* [2010] argued that possible differences may reach about 10% for the topography and gravity field corrections related to sediments. Both components contribute to the gravity noise, which effect is estimated by equation (2). The obtained results show that some limited areas of the platform are characterized by increased values of $\overline{\Gamma}^2_{F,I}$ (see below). These areas are excluded from the analysis.

4. Results

Maps of the effective elastic thickness for different values of the central wave number of the Morlet wavelet ($|\mathbf{k_0}| = 2.668, 3.081, 3.773,$ and 5.336) are shown in Figure 3. The gravity noise is relatively insignificant in most parts of the study area except in Africa, where the results are less reliable. Basically, all the maps demonstrate the same features, however with decreasing resolution, which is inversely proportional to the central wave number. We found that the two intermediate maps (Figures 3b and 3c) represent a reasonable compromise between the resolution and noise level. However, considering small-scale details in Figure 3b, one should take into account if they are reliable with respect to the noise level. On the other hand, the amplitude of the anomalies in Figure 3d ($|\mathbf{k_0}| = 5.336$) is already reduced due to smoothing.

In addition, we estimate the confidence intervals of T_e from the chi-square error distribution using standard errors of the observed coherence calculated from the jackknife method [*Kirby and Swain*, 2009; *Audet and Bürgmann*, 2011]. The T_e uncertainties corresponding to the 95% confidence intervals show that most of the study area is associated with low T_e uncertainties (less than 5 km). Larger errors are only found in the high T_e core of the eastern Arabian platform (about 5–20 km for the lowest $|\mathbf{k_0}|$); however, even in this case, they do not exceed 15% of the estimated values. The large uncertainties coincide with the zones of a high noise level (Figure 3), which are excluded from consideration.
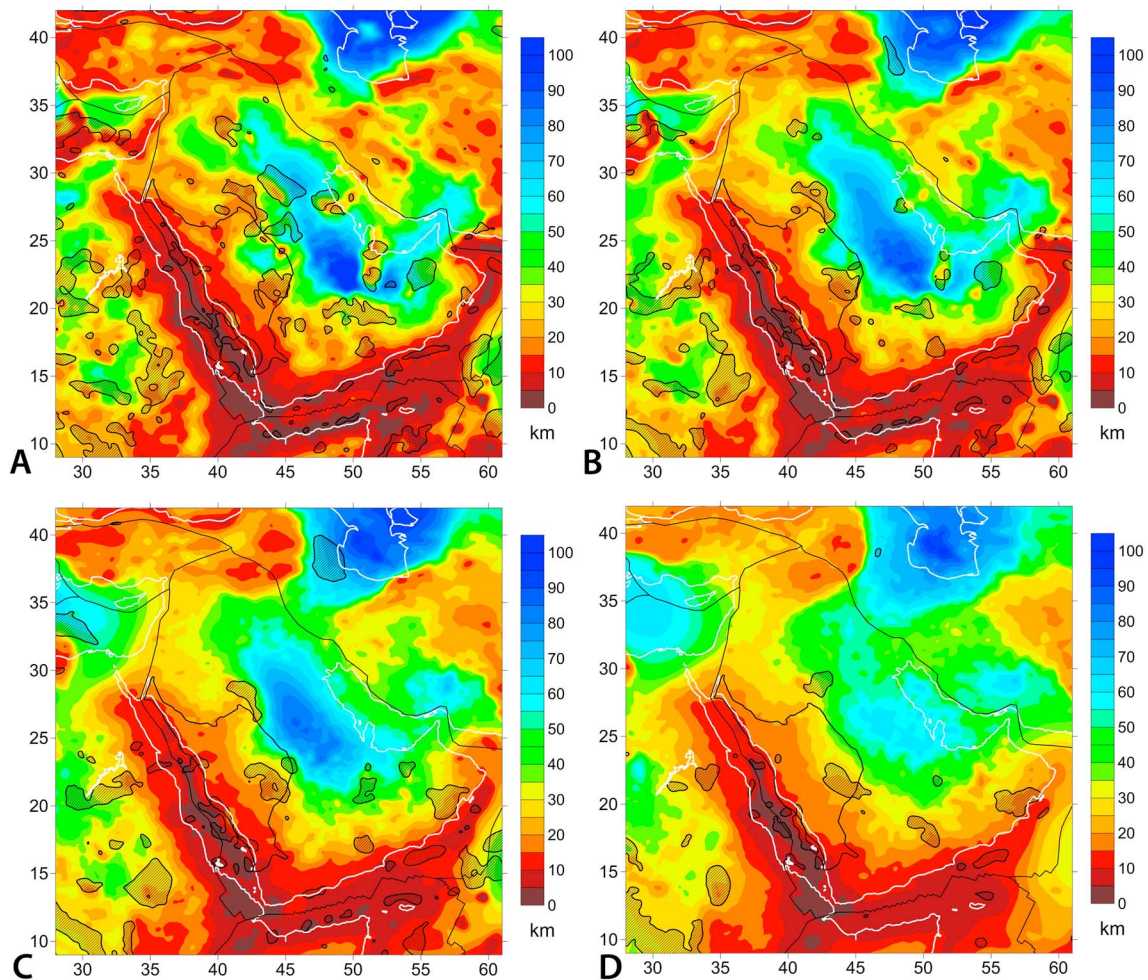
Figure 3. T_e for different values of the central wave number of the Morlet wavelet $|\mathbf{k_0}|$ = (a) 2.668, (b) 3.081, (c) 3.773, and (d) 5.336. The hatched patterns show the areas, where the maximum value of $\overline{\Gamma}^2_{F,l}$ (equation (2)) exceeds 0.5 and the results might be biased.

The obtained results generally correspond to the global results of *Audet and Bürgmann* [2011] and of *Pérez-Gussinyé et al.* [2009], however show many more details. In particular, it is clear that the anomaly in the western part of the Arabian shield is not a propagation of the rifting zone effect, since the weak zones are well resolved even on a small scale [*Kirby and Swain*, 2011]. The minimal T_e (3–10 km) corresponds to the rifting zones coinciding with the Gulf of Aden and Red Sea, which are the hottest zones within the study area. However, it should be noted that the bathymetry is partially based on altimetry data (although their contribution is likely not significant in the study area) [*Becker et al.*, 2009]; therefore, the results for the sea are less reliable. The western-southwestern part of the Arabian plate is also characterized by small to medium T_e (10–30 km), which normally corresponds to young tectonically active areas [e.g., *Audet and Bürgmann*, 2011; *Tesauro et al.*, 2013]. This zone well corresponds to the elevated topography (Figure 1a) except of the central part of the plate (eastern part of the Arabian shield), where a local maximum is found (T_e = 50–60 km). Localization of this anomaly is especially visible in the map for the minimal $|\mathbf{k_0}|$ (Figures 3a and 3b).

A significant part of the Arabian platform (especially the central one) is characterized by large values of T_e (50–75 km or more, with the possibility of greater thickness in the core), which are typical for old, cold, and tectonically inactive continental areas [e.g., *Audet and Bürgmann*, 2011; *Kirby and Swain*, 2009]. The amplitude of this anomaly could be even underestimated since its size is about the low limit for the fan wavelet method [*Kirby and Swain*, 2011]. The strong lithosphere is locally extended to the north (Lut Block) in the intersection of the Zagros suture zone and the Makran zone. Large values of T_e are also found in the
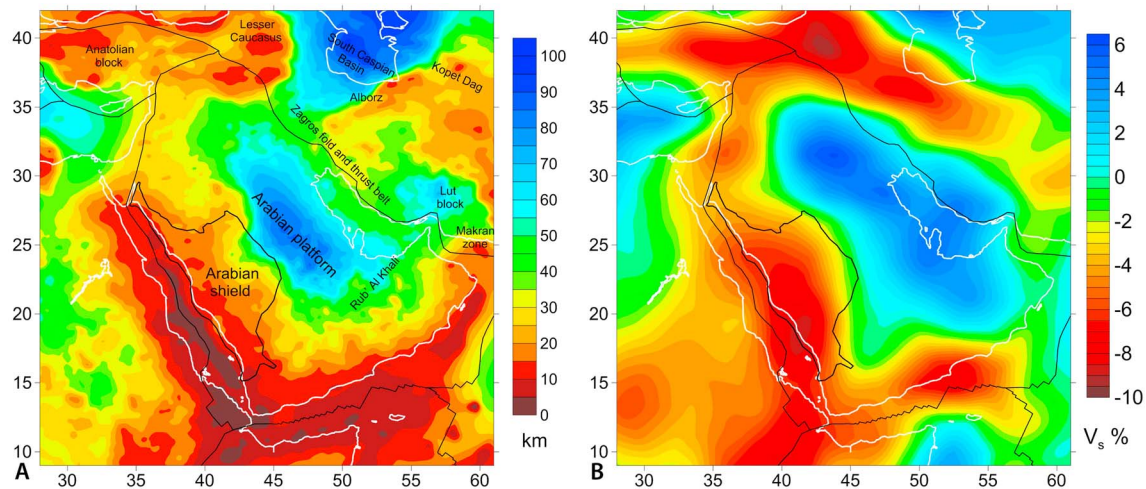
Figure 4. (a) Effective elastic thickness of the Arabian plate and surroundings, $|\mathbf{k_0}| = 3.773$. (b) V_s anomaly at a depth of 80 km [*Schaeffer and Lebedev*, 2013].

South Caspian Sea and surroundings. This zone has been already reported as a strong lithospheric block [*Jackson et al.*, 2002], which is supported by this study. The active orogenic belts in the northern part of the study area (Anatolian block, Lesser Caucasus, and partially Alborz) are characterized by low to intermediate T_e (10–30 km). Studies of physical parameters of the lithosphere evidence that these areas could be weakened due to thickening of the crust and to the effects of flexural stresses, caused by bending of the lithosphere under topographic and horizontal tectonic loads [e.g., *Burov and Diament*, 1995; *Tesauro et al.*, 2013]. Therefore, the lower crust becomes sufficiently hot, which leads to a significant decrease of the strength. This process also results in mechanical decoupling between the upper crust and the mantle lithosphere and in a large reduction of T_e [e.g., *Tesauro et al.*, 2013].

There exist several small-scale T_e anomalies (Figures 3a–3c). Particularly, a local minimum (~25 km) is found in the western part of the Rub' Al Khali basin. However, this area is also characterized by a high level of the gravity noise; therefore, the anomaly is likely artificial. It almost disappears already at $|\mathbf{k_0}| = 3.773$ and higher.

The calculated EET variations are generally in agreement with the recent seismic tomography model of *Schaeffer and Lebedev* [2013] (Figure 4). This model shows higher velocities in the upper mantle under the eastern part of the Arabian plate. However, according to the EET results, the strong lithosphere is confined to the Arabian platform, while it extends further to the northeast under the Zagros belt in the tomography model. We also do not see any seismic anomaly corresponding to the local EET maximum in the eastern part of the Arabian shield. Probably, these differences are due to the lower horizontal resolution of the tomography. However, it is also possible that other factors affect rigidity of the lithosphere in addition to temperature. This problem can be clarified by future high-resolution tomography studies.

5. Conclusions

1. We found a pronounced assymetry of the effective elastic thickness over the Arabian plate. The western part (chiefly the Arabian shield) is characterized by low to midvalues of EET (10–30 km) while the eastern one (the Arabian platform) by high values (~50 km and more in the core). This result confirms that the asymmetry of the topography is rather associated with fundamental structural differences of the lithosphere than with a forced tilt of the plate due to the rifting in the west-southwest and subduction in the northeast.
2. In agreement with seismic tomography, the variations of EET evidence that the eastern part should be much colder with a thick lithosphere comparing to the western part. Both the low EET and reduced V_s anomalies well correlate with the elevated topography over the plate; thus, we can assume that the uplift is supported by the hot mantle.
3. At the same time, we found many regional to local T_e anomalies, which show more complicated structure of the plate. The most prominent anomaly is observed in the eastern part of the Arabian shield, showing a relative maximum of the effective elastic thickness. This clearly demonstrates that T_e also depends on

many factors other than temperature variations within the lithosphere. In particular, it highly depends on coupling-decoupling conditions between crustal and lithospheric layers, which in turn depend on composition, stress conditions, and other factors.

References

Amante, C., and B. W. Eakins (2008), ETOPO1 1 arc-minute global relief model: Procedures, data sources and analysis, Natl. Geophys. Data Cent., NESDIS, NOAA, U.S. Dep. of Commer., Boulder, Colo., August 2008.

Audet, P., and R. Bürgmann (2011), Dominant role of tectonic inheritance in supercontinent cycles, *Nat. Geosci.*, *4*, 184–187, doi:10.1038/NGEO1080.

Audet, P., A. M. Jellinek, and H. Uno (2007), Mechanical controls on the deformation of continents at convergent margins, *Earth Planet. Sci. Lett.*, *264*(1), 151–166.

Becker, J. J., et al. (2009), Global bathymetry and elevation data at 30 arc seconds resolution: SRTM30_PLUS, *Mar. Geod.*, *32*(4), 355–371.

Braitenberg, C., Y. Wang, J. Fang, and H. Hsu (2003), Spatial variations of flexure parameters over the Tibet-Quinghai Plateau, *Earth Planet. Sci. Lett.*, *205*(3–4), 211–224, doi:10.1016/S0012-821X(02)01042-7.

Burov, E. B., and M. Diament (1995), The effective elastic thickness of (T_e) continental lithosphere: What does it really means?, *J. Geophys. Res.*, *100*, 3895–3904, doi:10.1029/94JB02460.

Chen, B., C. Chen, M. K. Kaban, J. Du, Q. Liang, and M. Thomas (2013), Variations of the effective elastic thickness over China and surroundings and their relation to the lithosphere dynamics, *Earth Planet. Sci. Lett.*, *363*, 61–72.

Chen, B., J. Liu, C. Chen, J. Du, and Y. Sun (2015), Elastic thickness of the Himalayan–Tibetan orogen estimated from the fan wavelet coherence method, and its implications for lithospheric structure, *Earth Planet. Sci. Lett.*, *409*, 1–14.

Förste, C., et al. (2013), EIGEN-6c3—A new combined global gravity field model including GOCE data up to degree and order 1949 of GFZ Potsdam and GRGS Toulouse, *Geophys. Res. Abstr. EGU Gen. Assembl.*, *15*, 4077–4081.

Forsyth, D. W. (1985), Subsurface loading estimates of the flexural rigidity of continental lithosphere, *J. Geophys. Res.*, *90*, 12,623–12,632, doi:10.1029/JB090iB14p12623.

Gettings, M. E., H. R. Blank Jr., W. D. Mooney, and J. H. Healey (1986), Crustal structure of southwestern Saudi Arabia, *J. Geophys. Res.*, *91*, 6491–6512, doi:10.1029/JB091iB06p06491.

Jackson, J., K. Priestley, M. Allen, and M. Berberian (2002), Active tectonics of the South Caspian Basin, *Geophys. J. Int.*, *148*(2), 214–245, doi:10.1046/j.1365-246X.2002.01588.x.

Kaban, M. K., and W. D. Mooney (2001), Density structure of the lithosphere in the southwestern United States and its tectonic significance, *J. Geophys. Res.*, *106*(B1), 721–739, doi:10.1029/2000JB900235.

Kirby, J. F., and C. J. Swain (2004), Global and local isostatic coherence from the wavelet transform, *Geophys. Res. Lett.*, *31*, L24608, doi:10.1029/2004GL021569.

Kirby, J. F., and C. J. Swain (2006), Mapping the mechanical anisotropy of the lithosphere using a 2D wavelet coherence, and its application to Australia, *Phys. Earth Planet. Inter.*, *158*(2), 122–138, doi:10.1016/j.pepi.2006.03.022.

Kirby, J. F., and C. J. Swain (2008), An accuracy assessment of the fan wavelet coherence method for elastic thickness estimation, *Geochem. Geophys. Geosyst.*, *9*, Q03022, doi:10.1029/2007GC001773.

Kirby, J. F., and C. J. Swain (2009), A reassessment of spectral T_e estimation in continental interiors: The case of North America, *J. Geophys. Res.*, *114*, B08401, doi:10.1029/2009JB006356.

Kirby, J. F., and C. J. Swain (2011), Improving the spatial resolution of effective elastic thickness estimation with the fan wavelet transform, *Comput. Geosci.*, *37*, 1345–1354, doi:10.1016/j.cageo.2010.10.008.

Koulakov, I. (2011), High-frequency P and S velocity anomalies in the upper mantle beneath Asia from inversion of worldwide traveltime data, *J. Geophys. Res.*, *116*, B04301, doi:10.1029/2010JB007938.

McKenzie, D. (2003), Estimating T_e in the presence of internal loads, *J. Geophys. Res.*, *108*(B9), 2438, doi:10.1029/2002JB001766.

Mooney, W. D., and M. K. Kaban (2010), The North American upper mantle: Density, composition, and evolution, *J. Geophys. Res.*, *115*, B12424, doi:10.1029/2010JB000866.

Pérez-Gussinyé, M., M. Metois, M. Fernández, J. Vergés, J. Fullea, and A. R. Lowry (2009), Effective elastic thickness of Africa and its relationship to other proxies for lithospheric structure and surface tectonics, *Earth Planet. Sci. Lett.*, *287*(1–2), 152–167.

Perotti, C. R., S. Carruba, M. Rinaldi, G. Bertozzi, L. Feltre, and M. Rahimi (2011), The Qatar–South Fars Arch Development (Arabian platform, Persian Gulf): Insights from seismic interpretation and analogue modelling, in *New Frontiers in Tectonic Research—At the Midst of Plate Convergence*, edited by U. Schattner, 364 pp., InTech, Rijeka, Croatia.

Schaeffer, A. J., and S. Lebedev (2013), Global shear-speed structure of the upper mantle and transition zone, *Geophys. J. Int.*, *194*(1), 417–449.

Stern, R. J., and P. Johnson (2010), Continental lithosphere of the Arabian plate: A geologic, petrologic, and geophysical synthesis, *Earth Sci. Rev.*, *101*, 29–67.

Stolk, W., M. K. Kaban, F. Beekman, M. Tesauro, W. D. Mooney, and S. Cloetingh (2013), High resolution regional crustal models from irregularly distributed data: Application to Asia and adjacent areas, *Tectonophysics*, *602*, 55–68.

Tesauro, M., M. K. Kaban, and S. A. P. L. Cloetingh (2013), Global model for the lithospheric strength and effective elastic thickness, *Tectonophysics*, *602*, 78–86.

Watts, A. B. (2001), *Isostasy and Flexure of the Lithosphere*, Cambridge Univ. Press, Cambridge, U. K.